Title
Capillary Surfaces in a Wedge: Differing Contact Angles

Authors
Concus, P.
Finn, R.

Publication Date
1993-04-01

LBL-33995
UC-405

Lawrence Berkeley Laboratory
UNIVERSITY OF CALIFORNIA

Physics Division

Mathematics Department

Presented at the International Symposium on Microgravity Science and Application, Beijing, China, May 10–13, 1993, and to be published in the Proceedings

Capillary Surfaces in a Wedge: Differing Contact Angles

P. Concus and R. Finn

April 1993

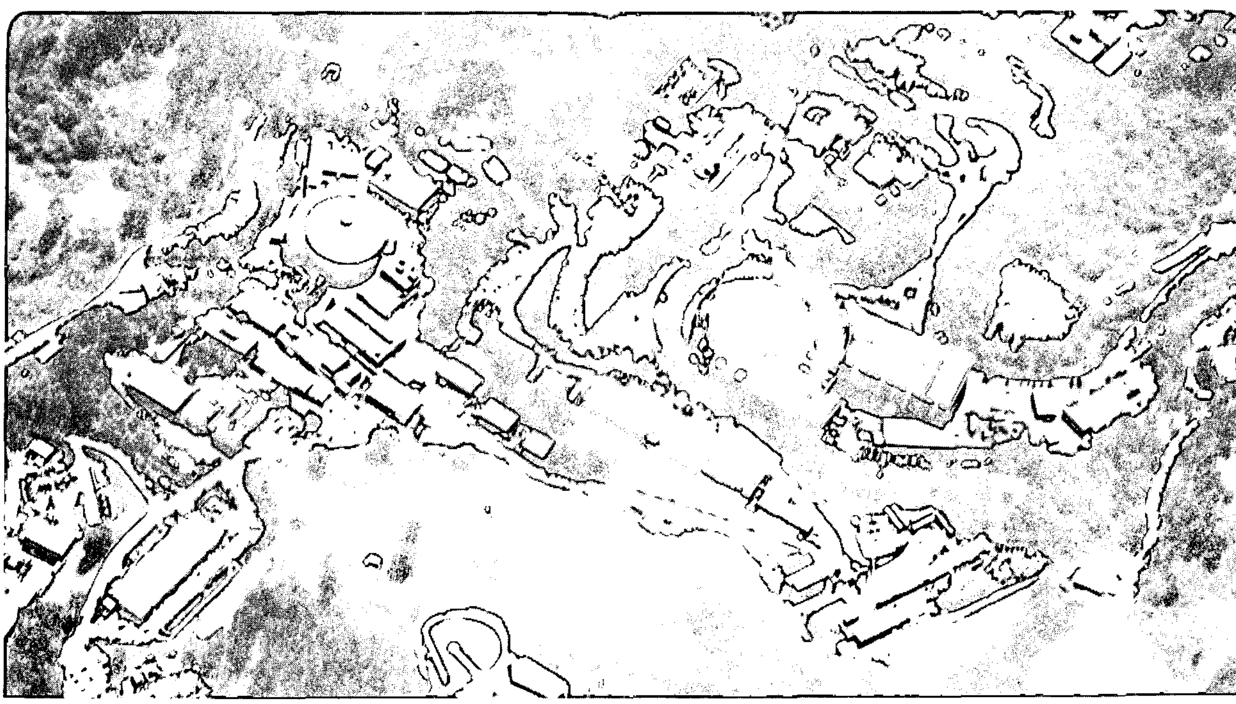

Prepared for the U.S. Department of Energy under Contract Number DE-AC03-76SF00098

DISCLAIMER

LBL-33995

CAPILLARY SURFACES IN A WEDGE: DIFFERING CONTACT ANGLES*

Paul Concus
Lawrence Berkeley Laboratory
and
Department of Mathematics
University of California
Berkeley, CA 94720

Robert Finn
Department of Mathematics
Stanford University
Stanford, California 94305

April 1993

*This work was supported in part by the Applied Mathematical Sciences Subprogram of the Office of Energy Research, U.S. Department of Energy, under Contract Number DE-AC03-76SF00098, by the National Aeronautics and Space Administration under Grant NAG3-1143, and by the National Science Foundation under Grant DMS89-02831.

CAPILLARY SURFACES IN A WEDGE: DIFFERING CONTACT ANGLES*

Paul Concus† and Robert Finn‡

Abstract

The possible zero-gravity equilibrium configurations of capillary surfaces $u(x, y)$ in cylindrical containers whose sections are (wedge) domains with corners are investigated mathematically, for the case in which the contact angles on the two sides of the wedge may differ. In such a situation the behavior can depart in significant qualitative ways from that for which the contact angles on the two sides are the same. Conditions are described under which such qualitative changes must occur. Numerically computed surfaces are depicted to indicate the behavior.

Introduction and Formulation

In an earlier note [1] we announced results concerning behavior of the free surface of a liquid partly filling a wedge container in the absence of gravity, when the contact angles on the two sides of the wedge are allowed to have different (constant) values. The mathematical results are presented in detail in [2]. Here we summarize the main findings and by means of numerically computed examples illustrate the physical behavior, which can differ markedly from that for the single-angle case.

We consider a cylindrical capillary tube in the absence of gravity with section Ω, closed at one end and partly filled with fluid forming a free surface $\mathcal{S}$. We suppose the boundary Σ of Ω to be piecewise smooth and to have an isolated corner P of opening 2α, $0 < 2\alpha < \pi$, forming a local "wedge domain" at P, see Fig. 1. We seek conditions under which, for prescribed constant (contact) angles γ_1 and γ_2 in the interval $[0, \pi]$, there will exist an $\mathcal{S}$ that can be (locally) represented by a function $z = u(x, y)$ over some neighborhood Ω^* of

* This work was supported in part by the Applied Mathematical Sciences Subprogram of the Office of Energy Research, U. S. Department of Energy, under Contract Number DE-AC03-76SF00098, by the National Aeronautics and Space Administration under Grant NAG3-1143, and by the National Science Foundation under Grant DMS89-02831.

† Lawrence Berkeley Laboratory and Department of Mathematics, University of California, Berkeley, CA 94720, U.S.A.

‡ Department of Mathematics, Stanford University, Stanford, CA 94305, U.S.A.

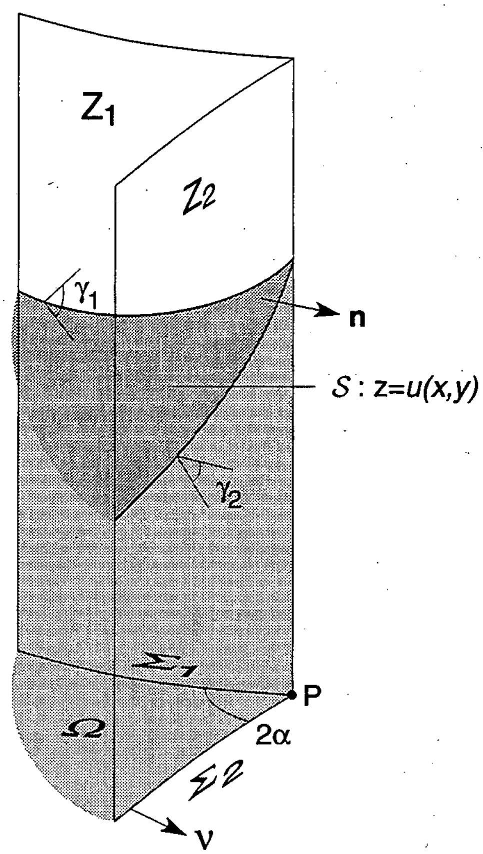

Fig. 1. The wedge configuration

P in Ω, and which meets the walls Z_1 and Z_2, over adjacent segments Σ_1 and Σ_2 of $\partial\Omega$ that abut at P, in the angles γ_1 and γ_2.

Specifically, we seek a solution of

$$\text{div } Tu = 2H \tag{1}$$

in some Ω^*, with

$$Tu = \frac{\nabla u}{\sqrt{1+|\nabla u|^2}} \tag{2}$$

and H an arbitrary prescribed constant, such that

$$\begin{aligned} \boldsymbol{\nu} \cdot Tu &= \cos\gamma_1 \quad \text{on } \Sigma_1 \\ \boldsymbol{\nu} \cdot Tu &= \cos\gamma_2 \quad \text{on } \Sigma_2, \end{aligned} \tag{3}$$

$\boldsymbol{\nu}$ being the unit exterior normal vector to Ω^* [3]. Geometrically, H is the *mean curvature* of $\mathcal{S}$; when $H = 0$, $\mathcal{S}$ becomes a minimal surface. In a physical situation, H is determined by the global configuration of Ω and by the boundary conditions over its entire boundary. One sees easily that meaningful physical conditions can give rise to any desired value of H. It is worth noting that if $\gamma_1 = \gamma_2 = \gamma$ over the entire boundary, then if $\gamma \neq \pi/2$ there holds $H \neq 0$; if $\gamma = \pi/2$, then the global problem admits the solution $u \equiv 0$ in Ω, which is unique up to an additive constant.

It is important to observe that in the statement of the problem, S is not assumed to be defined over P, and no growth conditions are imposed on $u(x, y)$ as P is approached from within Ω.

Previous Work

In earlier work [4, 5], we have shown that *for the equal-angle case* $\gamma_1 = \gamma_2 = \gamma$ *and for any constant* H, *a solution of* (1), (2), (3) *in any neighborhood of the vertex* P *can exist only if* $\frac{\pi}{2} - \alpha \leq \gamma \leq \frac{\pi}{2} + \alpha$ (the shaded interval in Fig. 2); *if* $H \neq 0$ *and if* Σ_1, Σ_2 *are linear segments* (Z_1 *and* Z_2 *are planes*), *then the condition is also sufficient, while if* $H = 0$ *then* $\frac{\pi}{2} - \alpha < \gamma < \frac{\pi}{2} + \alpha$ *suffices for existence.* Again we emphasize that no growth restriction is required at P. Tam [6] showed that *whenever a solution exists, then the surface* S *is continuous and has a continuous unit normal* $\mathbf{n}$ *up to* P, see also Miersemann [7] and Lieberman [8] for further developments. This remarkable behavior is the underlying reason that Vreeburg obtained in [9] the identical expression $\frac{\pi}{2} - \alpha \leq \gamma \leq \frac{\pi}{2} + \alpha$ as condition for existence of a surface with normal vector continuous to the vertex, without any use of the differential equation (1), (2), i. e., without reference as to whether or not the surface is a capillary surface.

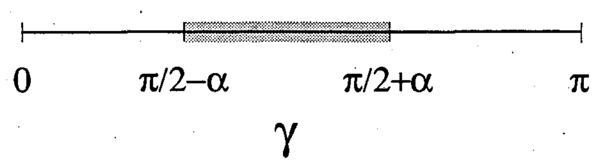

Fig. 2. Existence and non-existence intervals.

Subsequently Keller, King, and Merchant [10, §2] studied again the question of a capillary surface $u(x, y)$ defined in a wedge, with (possibly) differing angles γ_1, γ_2 on the two sides. They assume that the sides are planes extending to infinity and that the surface $u(x, y)$ extends to the entire infinite wedge with the same boundary condition; this is possible only in the particular case $H = 0$, thus limiting the physical interest of their discussion. Their paper has additional shortcomings, which are discussed in [2]. In both [9] and [10, §2], by unduly restricting the class of surfaces admitted into consideration, the authors eliminate from their studies solutions of the equation and boundary conditions that are mathematically (and also physically) significant. It is a curious accident that when the contact angles on the two wedge sides are equal, all the procedures lead to criteria that look formally similar. Despite the apparent similarities, the criteria do differ in an important way, even in that case. When differing contact angles on the two sides are contemplated, the distinctions become still more marked, and a whole range of solutions appears that is included neither in [9] nor in [10, §2]. The criteria for existence of these solutions are different from the ones established in those references, and lead in particular to different predictions as to results of experiments. It should be of considerable interest to design such experiments, which could be carried out in a suitable microgravity environment.

Mathematical Results

For the equal-angle case the explicit closed-form solution of a hemisphere for the wedge with planar sides provides a model to indicate the qualitative behavior in general. At $\gamma = \frac{\pi}{2} - \alpha$, the lower hemisphere, which is vertical over the vertex, yields a solution, for which $H > 0$. At $\gamma = \frac{\pi}{2} + \alpha$, the upper hemisphere does ($H < 0$). For γ interior to the shaded interval in Fig. 2, a lesser portion of a sphere than a hemisphere is a solution. Outside the interval no solution is possible. In general, for a solution in any wedge configuration the unit normal is horizontal (the surface becomes vertical over P) for the end points $\gamma = \frac{\pi}{2} - \alpha$ and $\gamma = \frac{\pi}{2} + \alpha$.

The results, derived in [2], that allow for differing contact angles can be described in terms of Fig. 3. The shaded rectangle $\mathcal{R}$ in the γ_1-γ_2 plane cuts off triangular domains $\mathcal{D}_1{}^+$, $\mathcal{D}_1{}^-$, $\mathcal{D}_2{}^+$, $\mathcal{D}_2{}^-$ in the $\pi \times \pi$ square, as indicated. The rectangle is inclined at 45° to

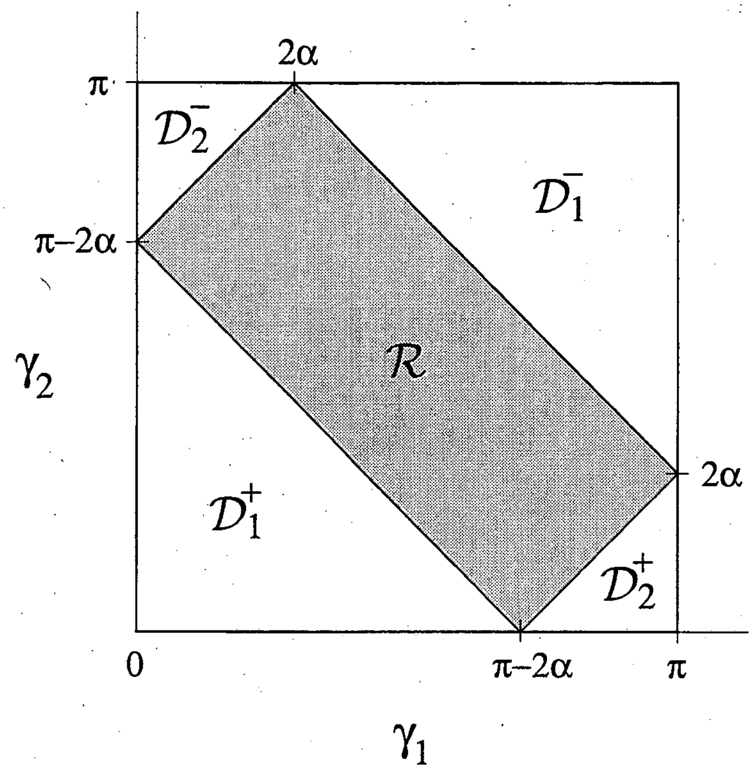

Fig. 3. Existence and non-existence regions.

the axes. In the statements of the results below, $\partial\mathcal{R} \cap \partial\mathcal{D}_1{}^+$ and $\partial\mathcal{R} \cap \partial\mathcal{D}_1{}^-$ refer to the interior of the specified edges of the rectangle (the corner points of $\mathcal{R}$, where $\mathcal{R}$ intersects the boundary of the $\pi \times \pi$ square, require special consideration). In [2] it is shown that:

(i) *A necessary condition for existence of a solution surface $\mathcal{S} : u(x, y)$ of* (1), (2), (3), *with unit normal* $\mathbf{n}$ *continuous up to P is that (γ_1, γ_2) lie in the closed rectangle $\mathcal{R}$ indicated in Fig.* 3*; the boundary of $\mathcal{R}$ corresponds to those configurations for which S is vertical* ($\mathbf{n}$ *horizontal) at P. If Σ_1 and Σ_2 are linear segments (Z_1 and Z_2 are planes), then if (γ_1, γ_2) lies interior to $\mathcal{R}$, a solution will exist, for any H; if $H > 0$ then a solution will exist when (γ_1, γ_2) lies on the boundary $\partial\mathcal{R} \cap \partial\mathcal{D}_1{}^+$, while if $H < 0$ then a solution will exist when (γ_1, γ_2) lies on the boundary $\partial\mathcal{R} \cap \partial\mathcal{D}_1{}^-$.*

(ii) *Any solution $u(x, y)$ corresponding to interior points of $\mathcal{R}$ or to $\partial\mathcal{R} \cap \partial\mathcal{D}_1{}^+$ or $\partial\mathcal{R} \cap \partial\mathcal{D}_1{}^-$ is continuous and admits a continuous unit normal vector up to P. For (γ_1, γ_2) lying in the regions $\mathcal{D}_1{}^+$ or $\mathcal{D}_1{}^-$ exterior to $\mathcal{R}$, no solution is possible.*

The above properties (i) and (ii) are straightforward generalizations of the equal-angle case (Fig. 2 shows the diagonal $\gamma_1 = \gamma_2$ of Fig. 3). The new features that can appear when $\gamma_1 \neq \gamma_2$ do so for values of (γ_1, γ_2) in $\mathcal{D}_2{}^+$ and $\mathcal{D}_2{}^-$:

(iii) *For (γ_1, γ_2) lying in the regions $\mathcal{D}_2{}^+$ or $\mathcal{D}_2{}^-$ exterior to $\mathcal{R}$, solutions of* (1), (2), (3) *may exist, but they cannot have continuous unit normal up to P.*

Examples of these last solutions for any α are provided by "moon-domain" surfaces, whose existence is proved in [11]. These surfaces have $\gamma_1 = 0$, $\gamma_2 = \pi$ on adjacent circular arcs of differing radius. The existence proof in [11] can be modified without essential change to extend to boundary data $\gamma_1 = \gamma$, $\gamma_2 = \pi - \gamma$, for any $0 \leq \gamma \leq \pi/2$ (Fig. 4). Thus one obtains a solution of the capillary problem for any value of γ; these solution surfaces have unit normal vectors discontinuous at P if γ is such that (γ_1, γ_2) lies outside the shaded rectangle $\mathcal{R}$ in Fig. 3. It can be shown that if $\gamma > 0$ then the surface is bounded above and below in Ω; if $\gamma = 0$ then $u(x, y) \to -\infty$ for any approach to the smaller circle, but remains bounded below on the larger one, and thus has an infinite jump discontinuity at P.

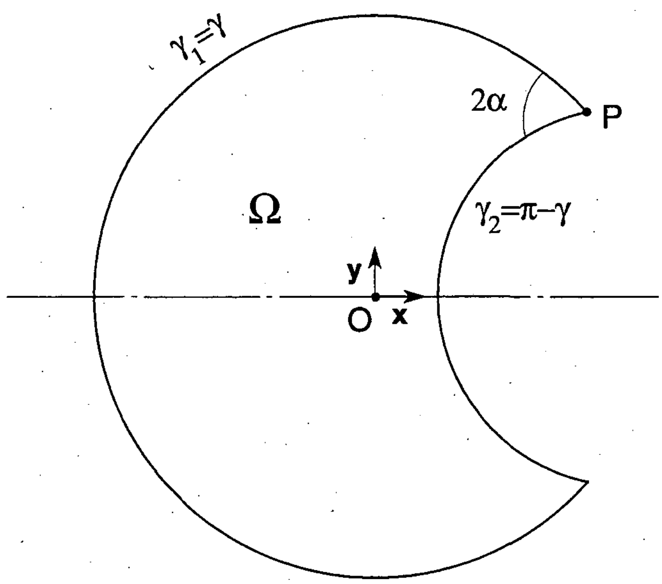

Fig. 4. Moon domain.

Thus, in a configuration with differing contact angles, solutions may appear whose behavior at P is very different from that which can occur in the equal-angle case. These solutions could not have been obtained by the procedures used for deriving results (i) and (ii).

Computed Surfaces

We illustrate with numerical examples the behavior that can be exhibited by solution surfaces with contact-angle values in $\mathcal{D}_2{}^+$ or $\mathcal{D}_2{}^-$. In these examples the numerical solutions of (1), (2), (3) are obtained using the adaptive-grid finite-element software package PLTMG [12]. The adaptive mesh refinement, which is based on computed $\mathcal{H}^1$ error estimates, permits the program to be effective even for non-smooth solutions. The mesh refinement and built-in graphical displays allow the user to infer the presence of discontinuities, such as those of interest for our problem, and permit a satisfactory numerical approximation to be obtained.

We take for the first example the moon domain depicted in Fig. 4. The radii of the larger and smaller circles are taken to be 1.5 and 1, respectively, with the centers located so that $2\alpha = 60°$. The computed surface $z = u(x, y)$ is shown in Fig. 5 for the three values $\gamma = 40°$, $20°$, and $10°$. For $\gamma = 40°$, the point (γ_1, γ_2) lies inside $\mathcal{R}$, and for $\gamma = 20°$ and $10°$, (γ_1, γ_2) lies inside $\mathcal{D}_2{}^-$. The boundary between the two domains corresponds to the critical value $\gamma = 30°$. The problem is solved numerically on the half-domain above the symmetry line $y = 0$ (Fig. 4), with the boundary condition that $\partial u/\partial \nu = 0$ on that line. The solutions are normalized to have $u = 0$ at the x-y origin O (the center of the larger circle). In Fig. 5 the surfaces are shown from a viewing position $x = 0, y = -1, z = 1$. The lowest point in the computed surfaces corresponds to the point at which the smaller circular arc in the moon-domain boundary intersects the symmetry line. The solution edge upward and to the left of the lowest point is the one over the symmetry line. The contour levels are depicted by shading, as indicated.

The difference between the behavior of the surfaces at P is readily seen. For $\gamma = 40°$ the solution appears to be smooth. In contrast, the $\gamma = 20°$ and $10°$ surfaces appear to have a jump discontinuity at P, substantially larger for $10°$ than for $20°$. These properties

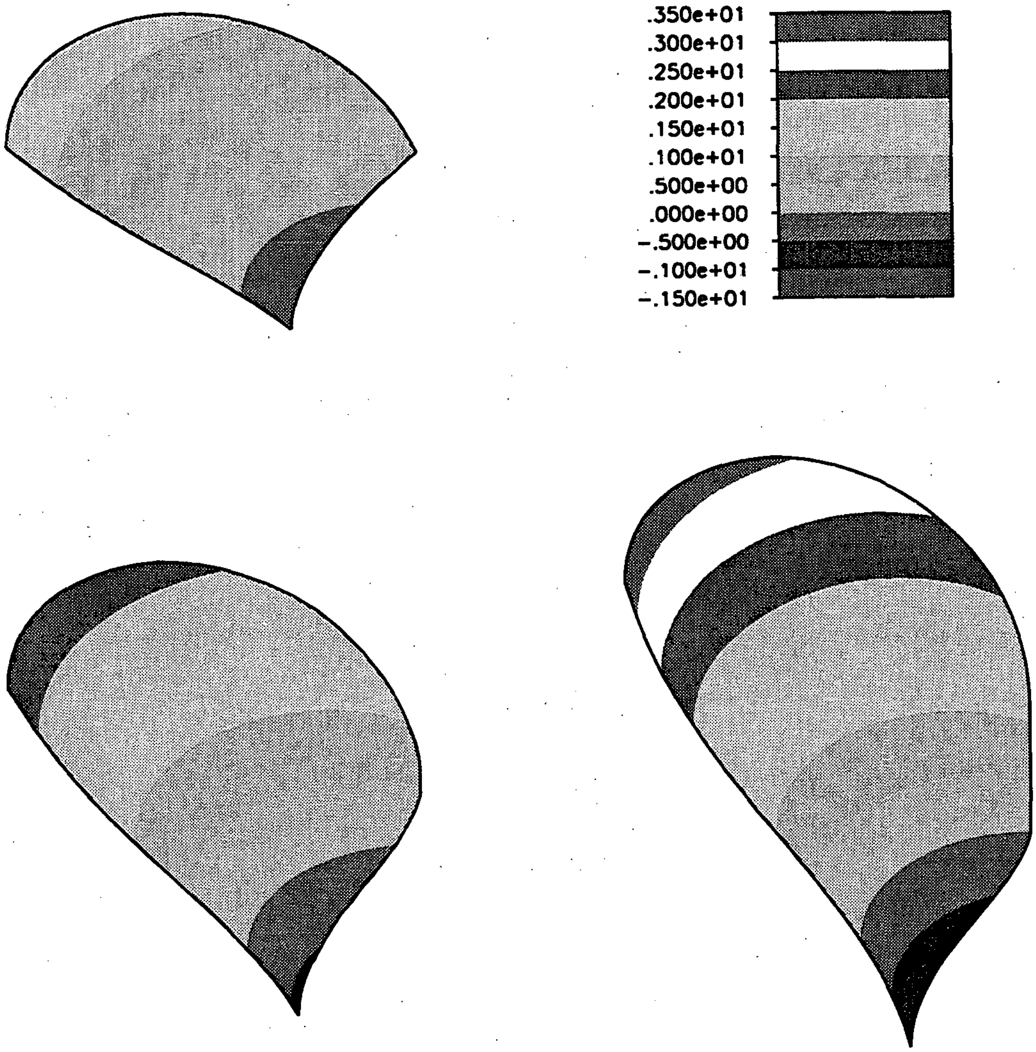

Fig. 5. Numerically computed solutions in the moon domain for $\gamma = 40°$ (upper left), $\gamma = 20°$ (lower left), and $\gamma = 10°$ (lower right).

were evidenced also by the behavior of the adaptive mesh refinement; for $\gamma = 40°$ the refinement was spread out over the domain, whereas for $\gamma = 20°$ and $10°$ the refinement, beyond a certain level, occurred only in successively smaller neighborhoods of P. The jump discontinuity for $10°$ is seen as being substantially larger than for $20°$; according to the mathematical results in [11], the discontinuity would become infinitely large as $\gamma \to 0$.

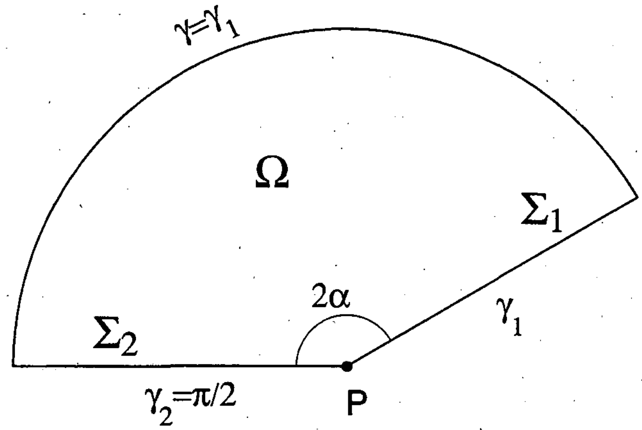

Fig. 6. Circular sector domain.

For the second example we solve (1), (2), (3) numerically for the circular sector domain shown in Fig. 6. We take $2\alpha = 150°$, $\gamma_2 = \frac{\pi}{2}$, and the contact angle on the circular arc to be γ_1, the same as that on Σ_1. Reference to Fig. 3 shows that a smooth solution can exist if γ_1 lies in the interval $60° < \gamma_1 < 120°$, but that a solution smooth up to P will not be possible for values outside the interval. The radius of the circular arc is taken to be 1.5. The solutions are normalized to have height $u = 0.1$ at $x = -.75, y = 0$, and are shown from a viewing point $x = 1, y = 0, z = 1$. (The x-y origin is at P, which is the center of the circle.)

Computed solution surfaces are shown in Fig. 7 for $\gamma_1 = 70°$ and for $\gamma_1 = 50°$. The surfaces are depicted in the larger boxes, and magnifications of the portions indicated in the smaller boxes enclosing a neighborhood of P are shown to the left. The surface height ranges only through the first few indicated contour intervals in these cases. For the $\gamma_1 = 70°$ case, the local behavior near P is seen to be smooth in accordance with the mathematical results ((γ_1, γ_2) lies inside $\mathcal{R}$). In contrast, for $\gamma_1 = 50°$ the surface can be

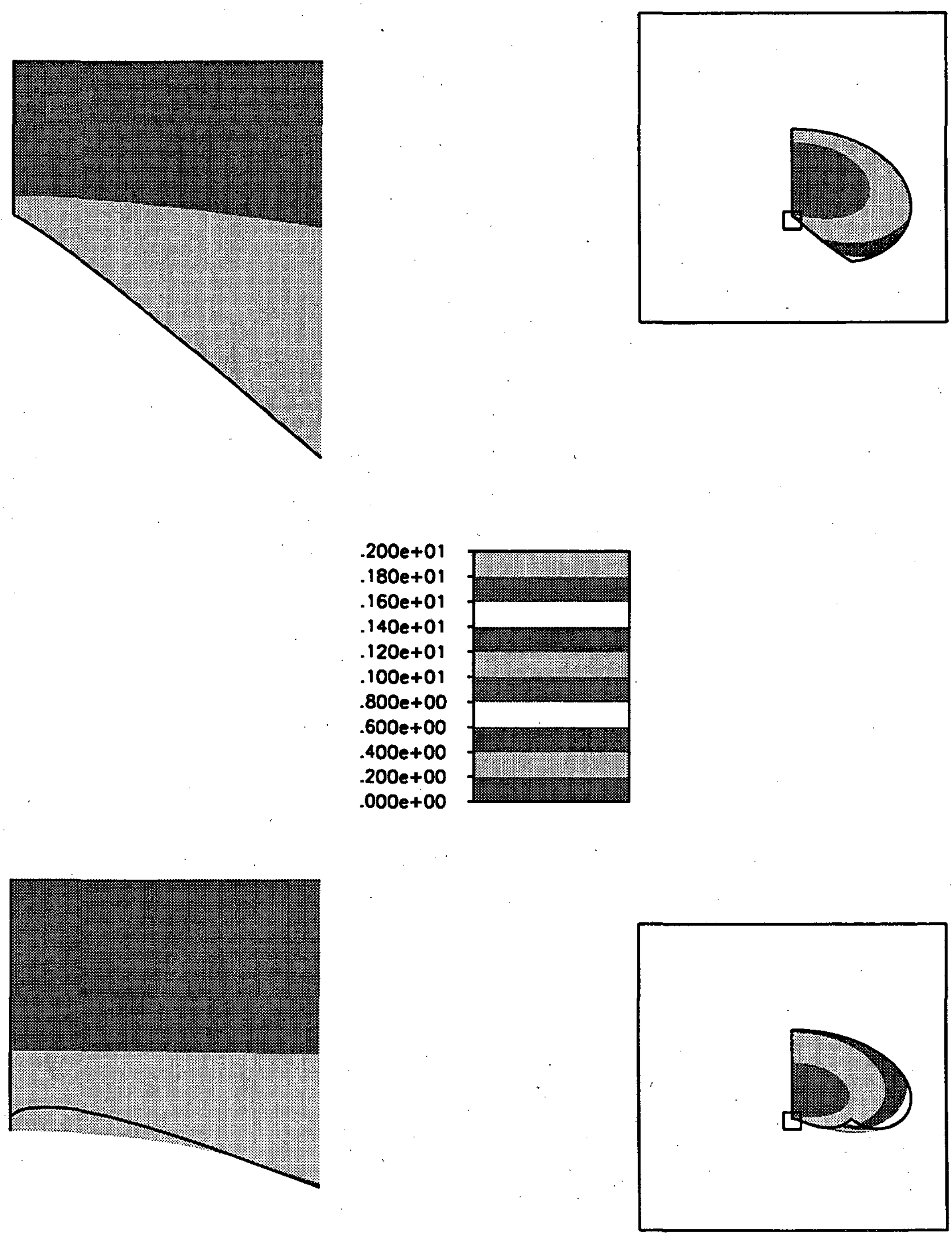

Fig. 7. Numerically computed solutions in the circular sector domain for $\gamma_1 = 70°$ (upper) and $\gamma_1 = 50°$ (lower).

seen to have a more complicated, non-smooth behavior at P. For this case the adaptive mesh refinement did not give evidence of a jump discontinuity in surface height at P, as it did for the moon surface example. A graphical display of the gradient vector did indicate a non-smooth behavior of the unit normal there, however. (At the other two corners of the domain, the behavior is smooth in accordance with the contact angle pairs lying inside $\mathcal{R}$ for both $\gamma_1 = 50°$ and $\gamma_1 = 70°$.)

By reflecting this example across Σ_2, one obtains an approximate solution in a circular sector with constant contact angle γ_1 on the entire boundary. This provides a connection between an example with differing contact angles and the case of a single contact angle for a domain with $2\alpha > \pi$. In a forthcoming work, Lancaster and Siegel characterize the local qualitative behavior of solutions at such corners [13]. Other numerically computed examples exhibiting discontinuous behavior at re-entrant corners for a single contact angle can be found in [14].

Concluding Remarks

The numerical experiments have indicated examples of capillary surfaces for particular γ_1, γ_2 pairs lying in the regions $\mathcal{D}_2{}^+$ or $\mathcal{D}_2{}^-$, and the non-smooth behavior exhibited by them at the wedge vertex. We conjecture that for any interior wedge angle 2α in the range $0 < 2\alpha < \pi$ considered, there exist wedge domains for which such solutions (with discontinuous normal) will exist for any γ_1, γ_2 pair in $\mathcal{D}_2{}^+$ or $\mathcal{D}_2{}^-$.

Acknowledgment

We wish to thank Victor Brady for carrying out the numerical solutions for the two test domains and for obtaining the graphical images shown in Figs. 5 and 7.

References

1. P. Concus and R. Finn: *On a comment by J.P.B. Vreeburg,* Microgravity Sci. Tech., IV (1991), p. 60.
2. P. Concus and R. Finn: *Capillary wedges revisited*, Preprint LBL-33553, Lawrence Berkeley Lab., Univ. of California, 1993 (submitted for publication).

3. R. Finn: Equilibrium Capillary Surfaces, Grundlehren 284, Springer-Verlag, New York, 1986.
4. P. Concus and R. Finn: *On capillary free surfaces in the absence of gravity,* Acta Math., 132 (1974), pp. 177–198.
5. P. Concus and R. Finn: *On the behavior of a capillary free surface in a wedge,* Proc. Nat. Acad. Sci. U.S.A., 63 (1969), pp. 292–299.
6. L.-F. Tam: *Regularity of capillary surfaces over domains with corners: borderline case,* Pacific J. Math., 124 (1986), pp. 469–482.
7. E. Miersemann: *On capillary free surfaces without gravity,* Z. Anal. Anwend., 4 (1985), pp. 429–436.
8. G. Lieberman: *Hölder continuity of the gradient at a corner for the capillary problem and related results,* Pacific J. Math., 133 (1988), pp. 115–135.
9. J.P.G. Vreeburg: *Comment on the paper "Parabolic flight experiments on fluid surfaces and wetting",* Microgravity Sci. Technol., III (1990), p. 125.
10. J.B. Keller, A. King, and G. Merchant: *Surface tension*, in Of Fluid Mechanics and Related Matters, Proc. Symp. for John Miles, Scripps Inst. Oceanography, Univ. of California at San Diego, 1991, pp. 161–168.
11. R. Finn: *Moon surfaces, and boundary behavior of capillary surfaces for perfect wetting and non-wetting,* Proc. Lon. Math. Soc., 57 (1988), pp. 542–576.
12. R.E. Bank: PLTMG: A Software Package for Solving Elliptic Partial Differential Equations, SIAM, Philadelphia, 1990; program available via *netlib* software distribution network.
13. K. Lancaster and D. Siegel: *Radial limits of capillary surfaces*, (to appear).
14. P. Concus, R. Finn, and F. Zabihi: *On canonical cylinder sections for accurate determination of contact angle in microgravity,* in Fluid Mechanics Phenomena in Microgravity, D.A. Siginer and M.M. Weislogel, eds., AMD–Vol. 154, Amer. Soc. Mech. Engineers, New York, 1992, pp. 125–131.

LAWRENCE BERKELEY LABORATORY
UNIVERSITY OF CALIFORNIA
TECHNICAL INFORMATION DEPARTMENT
BERKELEY, CALIFORNIA 94720